Solidification of binary alloys: Thermal effects studied with the phase-field model

M. Conti
Dipartimento di Matematica e Fisica, Universitá di Camerino, 62032 Camerino, Italy
(Received 25 June 1996)

We developed a phase-field model for solidification of binary alloys, accounting for thermal effects due to the release of latent heat at the solid-liquid interface. The model is utilized to study the planar growth of a solid germ nucleated in its undercooled melt. Steady state solutions, predicted by previous investigations in the isothermal limit, are lost, and the front velocity decays with time according to the diffusion power law $v \propto t^{-1/2}$. Due to the transient characteristics of the growth process, the solute segregation at the interface, as described by the present model, is substantially different from the predictions of the continuous growth model of Aziz and Kaplan [Acta Metall. **36**, 2335 (1988)], that is derived assuming isothermal and steady growth conditions. [S1063-651X(97)10601-8]

PACS number(s): 64.70.Dv, 68.10.Gw, 81.30.Bx, 82.65.Dp

I. INTRODUCTION

The interfacial dynamics in rapid solidification of binary alloys is addressed through sharp interface or diffuse interface models. Sharp interface models [1,2] utilize the diffusion equation to describe the transport of heat and solute through the bulk phases; the interface boundary conditions reflect two different constraints: (i) the energy and solute conservation across the moving front, and (ii) constitutive laws that relate the local interface conditions (concentration c and temperature T) to the front velocity v. Point (ii) requires a separate modelization of the interface kinetics on a microscopic scale, and was addressed by Aziz [3], Aziz and Kaplan [4], and Aziz and Boettinger [5] within the continuous growth model (CGM), assuming isothermal and steady growth conditions. They were able to explain the increase of the partition coefficient k (i.e., the ratio c_s/c_l of solute concentration in the growing solid to that in the liquid at the interface) from the equilibrium value k_e toward unity at large growth rates.

A diffuse interface approach to study alloy solidification is based on the phase-field model (PFM). A phase field $\phi(x,t)$ characterizes the phase of the system at each point; a free-energy (or entropy) functional, depending on ϕ, T, and c as well as on their gradients, is then extremized in respect to these variables, to derive the dynamic equations for the evolution of the process.

Wheeler, Boettinger, and McFadden (WBM1) [6] applied the PFM to alloy solidification, in the isothermal limit. They started from a free-energy functional that included a $(\nabla\phi)^2$ term. However, in their model the partition coefficient resulted in a decreasing function of the front velocity; this inconsistency, as pointed out by Wheeler, Boettinger, and McFadden (WBM2) [7] in a successive study, is due to the energy cost required to sustain large concentration gradients. To account for this effect, the model they developed included a $(\nabla c)^2$ term, acting to oppose the contraction of the solute profile at large velocities. Within this model, in the limit of steady growth, the solute segregation at the moving interface was properly described, and the results of the CGM were substantially recovered. Successively, in a numerical study, Conti [8] utilized the model to extend the analysis of the growth process to its transient stage, when the solute profile is not yet fully developed; in these conditions, the solute segregation at the interface did not fit the results of the continuous growth model.

All the previous studies were conducted neglecting thermal effects in the system. This approximation is commonly justified observing that, at least for metals, the latent heat released in the process is rejected away from the interface much faster than solute; thus the temperature field relaxes in times which are much shorter than the time required for rearrangement of chemical species, and solidification is effectively isothermal. Within this limit, starting from a uniformly undercooled melt $[c(x,0)=c_\infty]$, both the sharp interface model [2] and the phase-field model [7] show the possibility of a steady growth in the planar geometry, along a line in the v,T plane.

However, in a recent study, Karma and Sarkissian [9] pointed out that even for metals the latent heat released at the interface can significantly affect the dynamics of the phase-change process; successively Charach and Keizman [10], starting from an approximate formulation of the sharp interface model, in the limit of very dilute solutions, observed that, due to thermal effects, the steady growth of a planar germ should be driven into a diffusive regime. Then the effect of heat diffusion on the solidification of binary alloys is an interesting and still open question.

In the present study this point will be addressed simulating the planar growth of a solid germ with the phase-field model. It will be shown that due to the release of latent heat the interface temperature evolves with time, and the operating point that characterizes the process in the v,T plane is shifted from the steady growth line; the process enters the diffusive regime and the front velocity decays with time as $v \propto t^{-1/2}$.

The solute concentration jump at the interface increases with time, as predicted by the continuous growth model for a slowing front; however, due to the unsteady characteristics of the process, the solute segregation as described by the present model does not fit the picture given by the CGM.

The paper is organized as follows: in Sec. II a phase-field model will be developed that accounts for the evolution of the thermal field; the model will be utilized to study the

solidification of a nickel-copper ideal solution. In Sec. III some details of the numerical method will be given, and in Sec. IV the results of the numerical simulations will be presented. The conclusions will follow in Sec. V.

II. DEVELOPMENT OF THE MODEL

A. Derivation of the governing equations

The model improves the formulation given by WBM2 [7], allowing for the time evolution of the thermal field, and captures also many characteristics of the formulation given by Warren and Boettinger [11] in a successive study. The system is an initially undercooled binary alloy of components A (solvent) and B (solute). The entropy of the system is written as

$$\mathcal{S}=\int\left[s(e,\phi,c)-\frac{\epsilon^2}{2}|\nabla\phi|^2-\frac{\delta^2}{2}|\nabla c|^2\right]dv\,. \tag{1}$$

In Eq. (1), integration is performed over the system volume; $s(e,\phi,c)$ is the thermodynamic entropy density that depends on the internal energy density e and on the concentration and phase fields; the coefficients ϵ and δ account for the gradient term corrections. The phase field ϕ assumes the values $\phi=0$ in the solid and $\phi=1$ in the liquid; intermediate values correspond to the interface between the two phases. Conservation laws govern both solute and energy density transport:

$$\dot{e}=-\nabla\cdot\mathbf{J}_e, \tag{2}$$

$$\dot{c}=-\nabla\cdot\mathbf{J}_c\,. \tag{3}$$

The local entropy production is always positive if the energy and solute fluxes are written as

$$\mathbf{J}_e=M_e\nabla\frac{\delta\mathcal{S}}{\delta e}, \tag{4}$$

$$\mathbf{J}_c=M_c\nabla\frac{\delta\mathcal{S}}{\delta c}, \tag{5}$$

and the evolution of the phase field is given by

$$\dot{\phi}=M_\phi\frac{\delta\mathcal{S}}{\delta\phi}, \tag{6}$$

where M_e, M_c, and M_ϕ are positive constants.

In the above equations, the variational derivatives are given by

$$\frac{\delta\mathcal{S}}{\delta e}=\frac{\partial s}{\partial e}=\frac{1}{T}, \tag{7}$$

$$\frac{\delta\mathcal{S}}{\delta c}=\frac{\partial s}{\partial c}+\delta^2\nabla^2 c=\frac{\mu^A-\mu^B}{T}+\delta^2\nabla^2 c, \tag{8}$$

$$\frac{\delta\mathcal{S}}{\delta\phi}=\frac{\partial s}{\partial\phi}+\epsilon^2\nabla^2\phi. \tag{9}$$

In Eq. (8), μ^A and μ^B are the chemical potentials of the solvent and the solute; for an ideal solution we have

$$\mu^A=f^A(\phi,T)+\frac{RT}{v_m}\ln(1-c), \tag{10}$$

$$\mu^B=f^B(\phi,T)+\frac{RT}{v_m}\ln(c), \tag{11}$$

where R is the gas constant, and v_m is the molar volume; f^A and f^B are the free energy densities of the pure species A and B. To evaluate f^A, the internal energy density of pure A is postulated in the form

$$e^A(T)=e_s^A(T)+p(\phi)[e_l^A(T)-e_s^A(T)], \tag{12}$$

e_s^A and e_l^A being the internal energy densities in the solid and liquid phases, respectively; the function $p(\phi)$ is monotonically increasing from $p(0)=0$ in the solid to $p(1)=1$ in the liquid. Assuming constant and equal values for the specific heat C^A in both phases, the energy densities e_S^A and e_l^A are given by

$$e_s^A(T)=e_s^A(T_m^A)+C^A(T-T_m^A), \tag{13}$$

$$e_l^A(T)=e_l^A(T_m^A)+C^A(T-T_m^A), \tag{14}$$

where T_m^A is the melting temperature of pure A.

The difference

$$L^A=e_l^A(T_m^A)-e_s^A(T_m^A) \tag{15}$$

gives the latent heat per unit volume of species A. Then $f^A(\phi,T)$ can be written as

$$f^A=TG^A(\phi)+[e_s^A(T_m^A)-C^AT_m^A+p(\phi)L^A]\left(1-\frac{T}{T_m^A}\right)-C^AT\ln\left(\frac{T}{T_m^A}\right), \tag{16}$$

In Eq. (16) the function $G^A(\phi)$ is given by

$$G^A(\phi)=\tfrac{1}{4}W^A\phi^2(1-\phi)^2, \tag{17}$$

that is a symmetric double well potential with equal minima at $\phi=0$ and $\phi=1$, scaled by the positive well height W^A. With the choice $p(\phi)=\phi^3(10-15\phi+6\phi^2)$ the bulk solid and liquid are described by $\phi=0$ and $\phi=1$, respectively, for every value of temperature.

The free energy f^B is given by an equation similar to Eq. (16), with the material parameters labeled with the superscript A replaced with the ones related to the B species. The free energy of the solution is given by

$$f=(1-c)\mu^A+c\mu^B. \tag{18}$$

Using the thermodynamic equation

$$\frac{\partial s}{\partial\phi}=-\frac{1}{T}\frac{\partial f}{\partial\phi}, \tag{19}$$

Eqs. (6), (9), (10), (11), (16), (18), and (19) yield the dynamic evolution of the phase field as

$$\frac{\partial\phi}{\partial t}=M_\phi[\epsilon^2\nabla^2\phi-(1-c)H^A(\phi,T)-cH^B(\phi,T)], \tag{20}$$

where the function $H^A(\phi,T)$ is defined as

$$H^A(\phi,T)=G'(\phi)-p'(\phi)L^A\frac{T-T_m^A}{TT_m^A}, \tag{21}$$

and a similar expression holds for $H^B(\phi,T)$.

Starting from Eqs. (3), (5), and (8), and observing that

$$\nabla\frac{\mu^A-\mu^A}{T}=\frac{\partial}{\partial\phi}\frac{\mu^A-\mu^B}{T}\nabla\phi+\frac{\partial}{\partial c}\frac{\mu^A-\mu^B}{T}\nabla c+\frac{\partial}{\partial T}\frac{\mu^A-\mu^B}{T}\nabla T, \tag{22}$$

where

$$\frac{\partial}{\partial\phi}\frac{\mu^A-\mu^B}{T}=H^A(\phi,T)-H^B(\phi,T), \tag{23}$$

$$\frac{\partial}{\partial c}\frac{\mu^A-\mu^B}{T}=-\frac{R}{v_m}\frac{1}{c(1-c)}, \tag{24}$$

$$\frac{\partial}{\partial T}\frac{\mu^A-\mu^B}{T}=\Gamma(\phi,T), \tag{25}$$

with the function $\Gamma(\phi,T)$ defined as

$$\Gamma(\phi,T)=-\left[\frac{p(\phi)}{T^2}(L^A-L^B)+\frac{1}{T}(C^A-C^B)\right], \tag{26}$$

the dynamic equation for the concentration field is written as

$$\frac{\partial c}{\partial t}=-\nabla\cdot\left\{D_c c(1-c)\frac{v_m}{R}\nabla(\delta^2\nabla^2 c)+D_c c(1-c)\frac{v_m}{R}[H^A(\phi,T)-H^B(\phi,T)]\nabla\phi+D_c c(1-c)\frac{v_m}{R}\Gamma(\phi,T)\nabla T-D_c\nabla c\right\}. \tag{27}$$

In Eq. (26) we use the approximation $e_s^A(T_m^A)-C^AT_m^A=e_s^B(T_m^B)-C^BT_m^B$; in Eq. (27) the standard definition of the solute diffusivity D_c has been recovered, taking

$$D_c=\frac{M_c}{c(1-c)}\frac{R}{v_m}. \tag{28}$$

The evolution of the thermal field is easily derived from Eqs. (2), (4), (7), (12), and (15), taking $M_e=aT^2$ (a being the thermal conductivity of the alloy), and assuming $e(\phi,T)=(1-c)e^A(\phi,T)+ce^B(\phi,T)$:

$$\frac{\partial T}{\partial t}+[(1-c)L^A+cL^B]\frac{p'(\phi)}{C}\frac{\partial\phi}{\partial t}=D_T\nabla^2T. \tag{29}$$

Here and in the following the approximation is made $C^A=C^B=C$, and D_T is the thermal diffusivity of the alloy.

The model is then synthesized through Eqs. (20), (27), and (29). As the solute diffusivity is quite different in the solid and liquid phases, in the following D_c will be taken as

$$D_c=D_s+p(\phi)(D_l-D_s), \tag{30}$$

D_l and D_s being the diffusivities in the liquid and solid, respectively.

B. Nondimensional equations

The governing equations can be written in nondimensional form scaling lengths to some reference scale ξ, and time to ξ^2/D_l; the nondimensional temperature is defined as $u=C(T-T_m^A)/L^A$ and the functions $H^{A,B}(\phi,T)$ and $\Gamma(\phi,T)$ are scaled as $\tilde{H}^{A,B}(\phi,T)=(v_m/R)H^{A,B}(\phi,T)$ and $\tilde{\Gamma}(\phi,T)=(v_m/R)(L^A/C)\Gamma(\phi,T)$. We allow M_ϕ to depend on the local composition as

$$M_\phi=(1-c)M_\phi^A+cM_\phi^B, \tag{31}$$

and we introduce the following nondimensional parameters:

$$\tilde{L}=\frac{L^B}{L^A},\quad \tilde{\epsilon}^{A,B}=\frac{\epsilon}{\xi\sqrt{W^{A,B}}},$$

$$\tilde{D}=\frac{D_T}{D_l},\quad u^*=\frac{C(T_m^A-T_m^B)}{L^A},$$

$$m=\frac{M_\phi^B\epsilon^2}{D_l},\quad E=\frac{v_m}{R}\frac{\delta^2}{\xi^2},$$

$$\tilde{W}^{A,B}=\frac{v_m}{R}W^{A,B},\quad \alpha^{A,B}=\frac{L^{A,B}}{CT^\infty}\frac{L^{A,B}}{T_m^{A,B}}\frac{\xi^2}{\epsilon^2}\tilde{\epsilon}^{A,B},$$

$$n=\frac{M_\phi^A}{M_\phi^B}, \tag{32}$$

where T^∞ is the far-field temperature.

Then, if $(T-T^\infty)\ll T^\infty$, the nondimensional equations of the model become

$$\frac{\partial\phi}{\partial t}=[(1-c)n+c]m\nabla^2\phi-[(1-c)n+c]m\times\left\{(1-c)\left[\frac{G'(\phi)}{\tilde{\epsilon}^{A2}}-\frac{p'(\phi)\alpha^Au}{\tilde{\epsilon}^A}\right]+c\left[\frac{G'(\phi)}{\tilde{\epsilon}^{B2}}-\frac{p'(\phi)\alpha^B(u+u^*)}{\tilde{\epsilon}^B\tilde{L}}\right]\right\}, \tag{33}$$

$$\frac{\partial c}{\partial t}=\nabla\cdot\{\lambda(\phi)\nabla c-c(1-c)\lambda(\phi)\nabla(E\nabla^2 c)$$
$$-c(1-c)\lambda(\phi)[\tilde{H}^A(\phi,T)-\tilde{H}^B(\phi,T)]\nabla\phi$$
$$-c(1-c)\lambda(\phi)\tilde{\Gamma}(\phi,T)\nabla u\}, \quad (34)$$

and

$$\frac{\partial u}{\partial t}+[(1-c)+c\tilde{L}]p'(\phi)\frac{\partial\phi}{\partial t}=\tilde{D}\nabla^2 u, \quad (35)$$

where, in Eq. (34), $\lambda(\phi)$ is defined as

$$\lambda(\phi)=\frac{D_s}{D_l}+p(\phi)\left(1-\frac{D_s}{D_l}\right). \quad (36)$$

C. Numerical values of the parameters

The model parameters $\alpha^{A,B}$, $\tilde{\epsilon}^{A,B}$, $\tilde{W}^{A,B}$, m, and n were associated with the physical properties of the alloy components by WBM1 [6] and Warren and Boettinger [11]; below only the results are synthesized:

$$\alpha^{A,B}=\frac{L^{A,B}}{CT^\infty}\frac{\xi L_{A,B}}{6\sqrt{2}\sigma^{A,B}},\quad \tilde{\epsilon}^{A,B}=\frac{h^{A,B}}{\xi},$$

$$\tilde{W}^{A,B}=\frac{v_m}{R}\frac{12\sigma^{A,B}}{\sqrt{2}T_m^{A,B}h^{A,B}},\quad m=\frac{\beta^B\sigma^B T_m^B}{D_l L^B}, \quad (37)$$

$$n=\frac{\beta^A\sigma^A T_m^A L^B}{\beta^B\sigma^B T_m^B L^A},$$

where $\sigma^{A,B}$ is the surface tension of pure A or B; and $\beta^{A,B}$ is the kinetic undercooling coefficient, that relates the interface undercooling to the interface velocity through $v=\beta^{A,B}(T_m^{A,B}-T)$. In the phase-field model for a pure substance, the interface thickness is a free and independent parameter, that has been indicated in Eq. (37) through $h^{A,B}$. As ϵ is not allowed to depend on concentration, Eqs. (32) and (37) force the condition

$$\frac{h^B}{h^A}=\frac{\sigma^A T_m^B}{\sigma^B T_m^A}. \quad (38)$$

The gradient concentration coefficient δ, following the suggestion of WBM2 [7], will be chosen so that $\epsilon/\delta\ll 1$.

Table I summarizes the values of the thermophysical properties of nickel (A) and copper (B) utilized to estimate the above parameters [12]. The length scale was fixed at $\xi=2.1\times10^{-4}$ cm; a realistic value of h^A was selected as $h^A=1.68\times10^{-7}$ cm. With $\epsilon/\delta=8.75\times10^{-3}$, it results that $\alpha^A T^\infty/T_m^A=395.62$, $\alpha^B T^\infty/T_m^B=347.28$, $\tilde{\epsilon}^A=8.00\times10^{-4}$, $\tilde{\epsilon}^B=8.02\times10^{-4}$, $\tilde{W}^A=0.965$, $\tilde{W}^B=0.961$, $\tilde{D}=1.55\times10^4$, $\tilde{L}=0.735$, $m=350$, $n=1.01$, and $E=8\times10^{-3}$.

TABLE I. Material parameters for the Ni-Cu alloy.

	Nickel	Copper
T_m (K)	1728	1358
L (J/cm^3)	2350	1728
v_m (cm^3/mole)[a]	7.0	7.8
σ (J/cm^2)	3.7×10^{-5}	2.8×10^{-5}
β (cm/K s)[b]	160	198
D_l (cm^2/s)	10^{-5}	10^{-5}

[a]An average value of 7.4 will be taken.
[b]From the estimation of Willnecker *et al.* (Ref. [12]).

III. NUMERICAL METHOD

The evolution of Eqs. (33)–(35) has been considered in one spatial dimension, in the domain $-x_m\leqslant x\leqslant x_m$, with x_m large enough to prevent finite-size effects. We imposed the boundary conditions $\phi_x=c_x=T_x=0$ at the domain's walls. Initially in the undercooled melt, at uniform temperature and concentration T^∞ and c^∞, a solid germ is nucleated at the center of the domain at $x=0$; the germ thickness is the minimum required to prevent remelting and to ensure the successive growth. The germ composition was assumed to be $c(0,0)=c^\infty$. To discretize the equations, a second order in space and first order in time finite-difference approximations were utilized. Then an explicit scheme was employed to advance forward in time the phase field and concentration equations; the linear temperature equation was more conveniently integrated with a fully implicit method. To ensure an accurate spatial resolution, the computational domain was divided into two parts; in an inner region, of interest to the evolution of the phase and concentration fields, the grid spacing was selected as $\Delta x=0.5\tilde{\epsilon}$. In the outer region only the more diffuse temperature field changes with time; here a grid spacing $\Delta x=5\tilde{\epsilon}$ was utilized. A time step $\Delta t=0.25\times10^{-10}$ was required for numerical stability. To verify the consistency of the numerical scheme, at each time step both energy and solute conservation were checked. In all the simulations the energy balance was verified within 0.1%, and the mass balance within 0.001%.

IV. NUMERICAL RESULTS

The model presented above was proposed in its isothermal version by WBM2 [7]; they developed an asymptotic analysis for $\epsilon/\delta\ll1$, and solved in this limit the time independent equations. Given the far-field concentration, steady solutions were found for the growth process when the system temperature is below T_0, i.e., the temperature for which the Helmholtz free energy density has equal values in both phases. The same conclusions were recovered by Conti [8] for the long time solution of the fully time dependent equations.

In the present section the isothermal approximation will be relaxed; then the steady growth turns into a diffusive regime, with the interface velocity decaying with time as $v\propto t^{-1/2}$. Excepting for temperature, dimensionless units will be used throughout this section. The velocity scale is given by $v_0=D_l/\xi=4.76\times10^{-2}$ cm s^{-1}. Figure 1 shows, in the

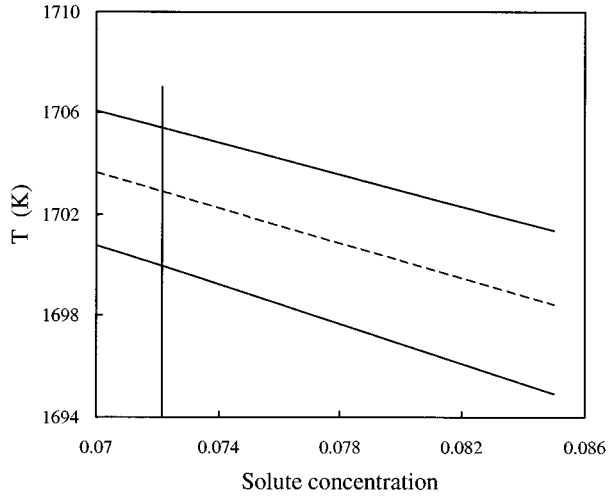

FIG. 1. A portion of the equilibrium phase diagram of the Ni-Cu alloy, computed from the data given in Table I. The vertical line corresponds to the value of c^{∞} used in the simulations. From top to bottom are represented the liquidus line, the T_0 line (dotted), and the solidus line.

(c,T) plane, the portion of the phase diagram of the alloy that will be explored in the following. The initial concentration of the melt is set to $c^{\infty}=0.072\,14$, that belongs to the solidus line at $T=1699.8$ K. Two values of the far-field temperature will be chosen to illustrate the numerical results, namely, $T^{\infty}=1695$ and 1700 K; in these conditions the isothermal model reaches long time steady solutions, with the front velocity given by $v=2.14\times10^{4}$ and 7.73×10^{3}, respectively. When the evolution of the thermal field is allowed through Eq. (35), a thermal gradient forms at the moving front, in order to diffuse away the latent heat; then the local temperature increases with time and the interface temperature and concentration no longer match the steady growth conditions. This behavior is shown in Fig. 2, where the interface temperature is represented versus time. The two curves start from different values of T^{∞}, below and above the solidus line at $c=c^{\infty}$; however, the operating point in both

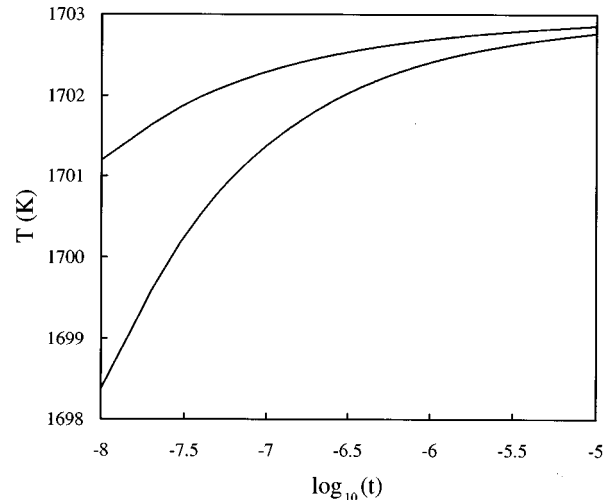

FIG. 2. Interface temperature vs time: $T^{\infty}=1700$ K (upper curve) and $T^{\infty}=1695$ K (lower curve).

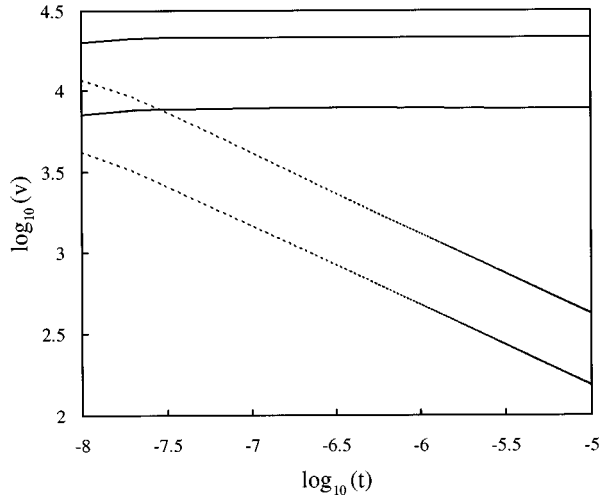

FIG. 3. Interface velocity vs time. Solid lines: isothermal approximation ($T^{\infty}=1695$ and 1700 K, from top to bottom); dotted lines: present model ($T^{\infty}=1695$ and 1700 K, from top to bottom).

cases evolves into the region of the phase diagram confined between the liquidus and solidus lines, and the initial difference is reabsorbed with time; this result is in agreement with some first calculations based on the sharp interface model, that show, in the very dilute solution limit, that the final state does not depend on the initial melt temperature [10].

For the same values of T^{∞}, Fig. 3 shows the interface velocity versus time (dotted lines); to accommodate the reader, the steady solutions of the isothermal limit are also plotted in the graph (solid lines). The log-log plot indicates that for the present model the front velocity scales with the familiar diffusive law $v\propto t^{-1/2}$.

In Fig. 4 we display the temperature field sampled at three different times, for $T^{\infty}=1700$ K; the curves show the progressive spreading of the thermal field. The effect is characteristic of the diffusive growth, as the interface velocity decays with time, and correspondingly the characteristic length of the thermal field D_T/v increases.

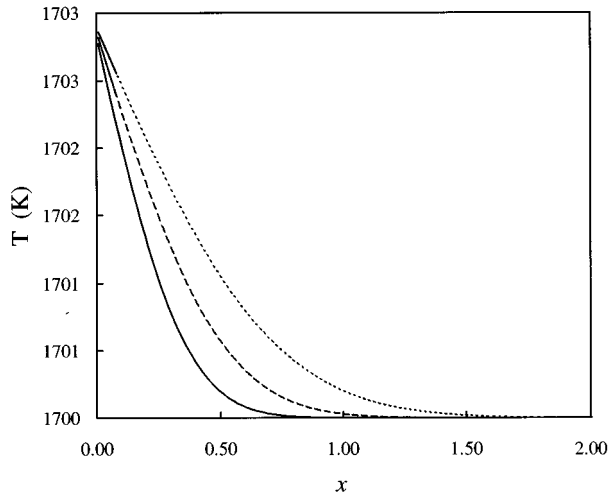

FIG. 4. Temperature profiles at three different times: $t=2.5\times10^{-6}$ (solid line), 5.0×10^{-6} (dashed line), and 9.0×10^{-6} (dotted line). $T^{\infty}=1700$ K.

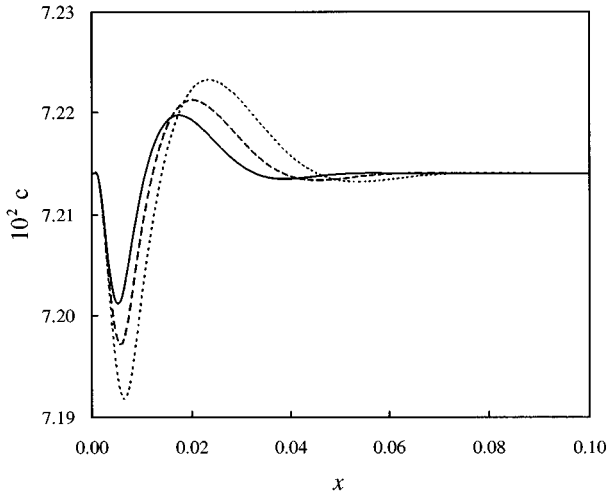

FIG. 5. Concentration profiles at three different times: $t=2.5\times10^{-6}$ (solid line), 5.0×10^{-6} (dashed line), and 9.0×10^{-6} (dotted line). $T^{\infty}=1700$ K.

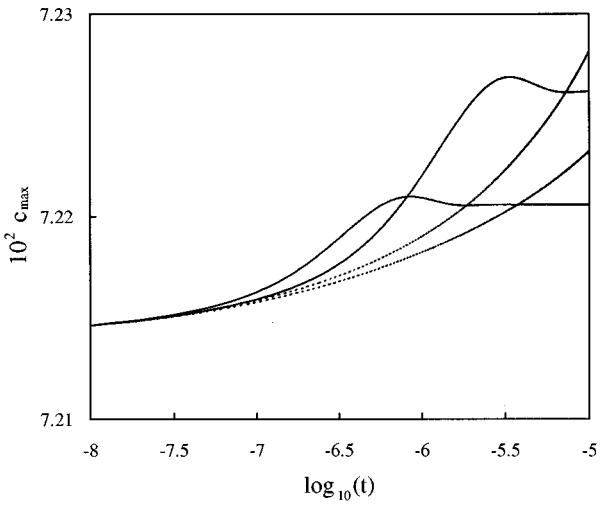

FIG. 6. Solute concentration on the liquid side of the interface, vs time. Solid lines: isothermal approximation ($T^{\infty}=1700$ K and $T^{\infty}=1695$ K, from top to bottom); dotted lines: present model ($T^{\infty}=1695$ K and $T^{\infty}=1700$ K, from top to bottom).

The solute concentration field, sampled at the same times, is shown in Fig. 5 for the same value of T^{∞}. The $(\nabla c)^2$ correction in the entropy functional (1) penalizes the growth of large concentration gradients; as shown by the curves, the concentration jump across the interface develops along a characteristic length of the order of 10^{-2}, that is much larger than the length scale of the phase-field transition. The damped oscillation of the profile ahead of the interface is due to the fourth order diffusion equation, and is not expected for the classical second order diffusion problem [7].

The continuous growth model [3–5], that is developed within the isothermal approximation and assumes steady growth, predicts a monotonic increase of the partition coefficient k with the front velocity; the functional form of k can be given by

$$k(v)=\frac{k_e+v/v_d}{1+v/v_d}, \tag{39}$$

where v_d is a characteristic kinetic velocity which is often taken as D_l/a_0, a_0 being an interatomic dimension. Equation (39) reduces to $k=k_e$ at equilibrium (maximum segregation), and describes the progressive suppression of solute segregation ($k\rightarrow1$) at large interface velocities.

Although the present data refer to a slowing front, the curves shown in Fig. 5 are in qualitative agreement with the predictions of the CGM: as time elapses, the front velocity decays and the concentration jump at the interface increases, i.e., k decreases. However, a finite relaxation time is necessary to develop the solute profile, and the latter cannot follow instantaneously the time variation of the front velocity; as a result the concentration jump given by Eq. (39) is larger than the actual one, shown in Fig. 5. At $t=9\times10^{-6}$ the dotted line indicates a value of $k=0.99$, while Eq. (39) would give $k=0.93$ (8).

To evaluate the solute segregation on the moving front, we computed the maximum value $c_{\max}$ of $c(x,t)$, that identifies the concentration c_l on the liquid side of the interface; on the solid side we associated the concentration c_s to the value of $c(x,t)$ corresponding to $\phi(x,t)=0.05$.

Figure 6 shows $c_{\max}$ for $T^{\infty}=1695$ and 1700 K (dotted lines, upper and lower curves, respectively); the solid lines indicate the solutions computed from the isothermal model ($T^{\infty}=1700$ and 1695 K, from the top to bottom). The solute segregation reflects the unsteady characteristics of the process. The isothermal curves of Fig. 6 show that the relaxation time t^* of the solute peak becomes shorter as the growth rate increases. As a consequence, in the isothermal approximation during the first transient solute, partitioning is more effective at large growth rates; at long times, as expected, lower values of $c_{\max}$ correspond to higher values of the front velocity.

The dotted lines indicate that in the present model increasing the far-field temperature (i.e., decreasing the growth rate) results in lower values of $c_{\max}$; then the solute segregation would be more effective at higher velocities. This appearent paradox is easily explained referring to the above considerations: as t^* is comparable with the relaxation time of the temperature field, the short time features of the solution survive along the growth process.

V. CONCLUSIONS

Rapid solidification of binary alloys is generally addressed in the isothermal approximation, due to the large ratio of heat to solute diffusivity. Within this approximation both the continuous growth model and the phase-field model admit steady solutions for the growth in planar geometry. In this paper it has been shown that even for metals the effects due to the evolution of the thermal field cannot be neglected. The steady growth regime predicted by previous studies is turned into a diffusive regime, with the front velocity decaying with time as $v\propto t^{-1/2}$. The relaxation times of the thermal and concentration fields are comparable, and the solute concentration at the interface cannot instantaneously follow the local temperature and velocity conditions. Then the solute segregation, as described by the present model, reflects the unsteady characteristics of the process, and does not fit the predictions of the continuous growth model.

[1] Ch. Charach and B. Zaltzman, Phys. Rev. E **49**, 4322 (1994).
[2] Ch. Charach and Y. Keizman, in *Computational Modelling of Free and Moving Boundaries Problems*, edited by L. C. Wrobel, B. Sarler, and C. A. Brebbia (Computational Mechanics Publications, Southampton, 1995).
[3] M. J. Aziz, J. Appl. Phys. **53**, 1158 (1982).
[4] M. J. Aziz and T. Kaplan, Acta Metall. **36**, 2335 (1988).
[5] M. J. Aziz and W. J. Boettinger, Acta Metall. **42**, 527 (1994).
[6] A. A. Wheeler, W. J. Boettinger, and G. B. McFadden, Phys. Rev. A **45**, 7424 (1992).
[7] A. A. Wheeler, W. J. Boettinger, and G. B. McFadden, Phys. Rev. E **47**, 1893 (1993).
[8] M. Conti (unpublished).
[9] A. Karma and A. Sarkissian, Phys. Rev. E **47**, 513 (1993).
[10] Ch. Charach and Y. Keizman (private communication).
[11] J. A. Warren and W. J. Boettinger, Acta Metall. Mater. **43**, 689 (1995).
[12] R. Willnecker, D. M. Herlach, and B. Feuerbacher, Phys. Rev. Lett. **62**, 2707 (1989).